*Journal of the European Ceramic Society* **10** (1992) 33–40

# Weakest-link Failure Prediction for Ceramics II: Design and Analysis of Uniaxial and Biaxial Bend Tests

H. Scholten, L. Dortmans, G. de With*

Centre for Technical Ceramics, PO Box 595, 5600 MB Eindhoven, The Netherlands

&

B. de Smet, P. Bach

Netherlands Energy Research Foundation, PO Box 1, 1755 ZG Petten, The Netherlands

(Received 22 July 1991; accepted 5 November 1991)

***Abstract***

*Two uniaxial (three- and four-point) bend tests and two biaxial (ball-on-ring and ring-on-ring) bend tests for ceramics have been analysed. Experimental and numerical concepts are presented which are necessary to obtain reliable test results and which allow for the extrapolation of uniaxial to biaxial strength data. A corresponding experimental accuracy has been achieved at two different laboratories for a justified exchange of these data.*

*Zwei uniaxiale Biegeversuche (Drei-Punkt- und Vier-Punkt-Biegeversuch) und zwei biaxiale Biegeversuche (Kugel-auf-Ring- und Ring-auf-Ring-Biegeversuch) für keramische Werkstoffe wurden analysiert. Es werden experimentelle und numerische Konzepte vorgestellt, die eine Extrapolation von uniaxialen zu biaxialen Festigkeitsdaten ermöglichen und die für zuverlässige Testergebnisse Voraussetzung sind. Die entsprechende experimentelle Genauigkeit für einen gerechtfertigten Austausch dieser Daten wurde an zwei verschiedenen Laboratorien erreicht.*

*Deux tests uniaxiales (trois et quatre points) et deux tests biaxiales de flexion (bille sur anneau et anneau sur anneau) pour céramiques ont été analysés. Des concepts expérimentaux et numériques sont présentés, qui sont nécessaires pour obtenir des résultats fiables et qui permettent l'extrapolation des données uniaxiales en données biaxiales de résistance mécanique. Une justification expérimentale correspondante a été réalisée dans deux laboratoires différents pour justifier l'échange de ces données.*

## 1 Introduction

Bend tests, both uniaxial and biaxial, are widely used to determine the strength of ceramics. Besides simple shapes to machine, a main advantage of these tests is the elimination of alignment and gripping problems occurring in pure tensile tests.

It is well known that bend tests suffer from their own problems as well. The uniaxial (three- and four-point) bend tests have been the subject of detailed studies which describe several possible errors, due to which stress calculations from applied loads can be severely in error.[1–4] The main errors are friction at the specimen supports, wedging, twisting and alignment errors. Similar remarks can be made for the biaxial (ball-on-ring and ring-on-ring) bend tests. In the case of ball-on-ring loading, the correct solution for the constant stress zone has been discussed.[5–7] Correct ring-on-ring loading has been shown to be difficult to realize, since solid toroid rings are likely to introduce friction into the bending system.[8–10]

For the prediction of biaxial strength from uniaxial data, a high experimental accuracy, within one or two per cent, is a prerequisite. It has also been shown[11] that, without this accuracy, strongly biased Weibull parameters can result for higher values of the Weibull modulus $m$.

* Also affiliated with Philips Research Laboratories, PO Box 80000, 5600 JA Eindhoven, The Netherlands.



*Journal of the European Ceramic Society* 0955-2219/92/$05.00 

**Table 1.** Experimental configurations

| *Laboratory* | *Jig* | *Test* | *Material* | *Strain gauge* | *v (mm/min)* | *N* |
|---|---|---|---|---|---|---|
| CTK | A | 3P20 | Borosilicate glass | 3 | 0·063 | 7 |
| | | 3P30 | | | 0·100 | 7 |
| | | 3P40 | | | 0·100 | 7 |
| | | 4P | | | 0·100 | 2 |
| | B | BOR6PS | Crown glass | 1, 2, 3, 4 | 0·025 | 12 |
| | | BOR6BS | | | 0·025 | 8 |
| | | BOR10BS | | | 0·050 | 12 |
| | C | ROR | Crown glass | 1, 2, 3 | 0·085 | 9 |
| ECN | D | 3P20 | Borosilicate glass | 3 | 0·100 | 1 |
| | | 3P30 | | | 0·100 | 1 |
| | | 3P40 | Borosilicate glass, alumina | 3, 5 | 0·100 | 2·2 |
| | E | 4P | Borosilicate glass, alumina | 3, 5 | 0·100 | 2·2 |
| | F | 4P | Alumina | 5 | 0·100 | 1 |

A = Three-point bend jig; B = ball-on-ring jig; C = ring-on-ring jig; D = three-point bend jig; E = four-point bend jig (Nimonic); F = four-point bend jig (SiC); $N$ = number of measurements; $v$ = crosshead speed; strain gauge numbers refer to Table 3. 3P20, 3P30, 3P40 = three-point bend tests at span lengths of 20, 30 and 40 mm respectively; 4P = four-point bend test (inner span length = 20 mm; outer span length = 40 mm); BOR6PS = ball-on-ring test on pin support, 6 mm in radius; BOR6BS, BOR10BS = ball-on-ring test on ball-bearing support of 6 and 10 mm in radius respectively; ROR = ring-on-ring test (inner ring 6 mm, outer ring 10 mm in radius).

In the present work, the performance of four uniaxial and two biaxial bending jigs at two different laboratories has been investigated by strain gauge measurements. A main objective was to achieve the earlier mentioned accuracy, which is a prerequisite for the compatibility of strength tests performed at different laboratories. For each experiment, the measured force–strain relationships were used to compute the Young's modulus of the material. These values in turn were compared to Young's moduli obtained by the pulse-echo technique, the latter being considered as a reference value. Deviations yield information about errors in the bend tests.

## 2 Experimental Procedure

Several uniaxial and biaxial bend jigs, listed in Table 1, were designed and tested. The materials and their properties, together with the dimensions of the specimens are listed in Table 2. The jigs A, B and C were designed and tested at the Centre for Technical Ceramics (CTK), D, E and F at the Netherlands Energy Research Foundation (ECN).

Jigs A and D (Fig. 1(a)) were quite similar and easily convertible for three-point bending at different span lengths. The main difference was that jig A could also be converted for four-point bending. In both lower and upper blocks of these jigs, slightly oversized flat grooves were milled, resulting in a clearance of 0·2 mm. Thus, the rollers were able to move during bending. The bending experiments were carried out by placing the rollers to the inner and outer edges of these grooves. The exact roller distances were taken into account during subsequent calculations. For the three-point bend experiments the loading roller was placed in a central V-groove within the upper block. The diameter of both the loading and support rollers was

**Table 2.** Materials and properties

| | *Borosilicate glass* | *Alumina*[a] | *Crown glass* |
|---|---|---|---|
| Density (g/cm$^3$) | 2·21 | 3·85 | 2·51 |
| Young's modulus,[a] $E$ (GPa) | 61·6 | 369 | 71·3 |
| Poisson's ratio[a] | 0·189 | 0·237 | 0·221 |
| Shape | bar | | disc |
| Dimensions (mm) | length 50·0 ± 0·1 | | diameter 15·0 ± 0·1 |
| | width 3·5 ± 0·1 | | width 10·0 ± 0·1 |
| | height 4·5 ± 0·1 | | thickness 1·0 ± 0·1 |
| Roughness $R_a$ ($\mu$m) | < 0·3 | | < 0·3 |
| Flatness ($\mu$m) | < 5 | | < 5 |
| Plane parallelism ($\mu$m) | < 5 | | < 5 |

[a] Calculated from the usual formulae using pulse-echo with longitudinal waves at 5 MHz and transverse waves at 20 MHz. No correction for damping was applied.

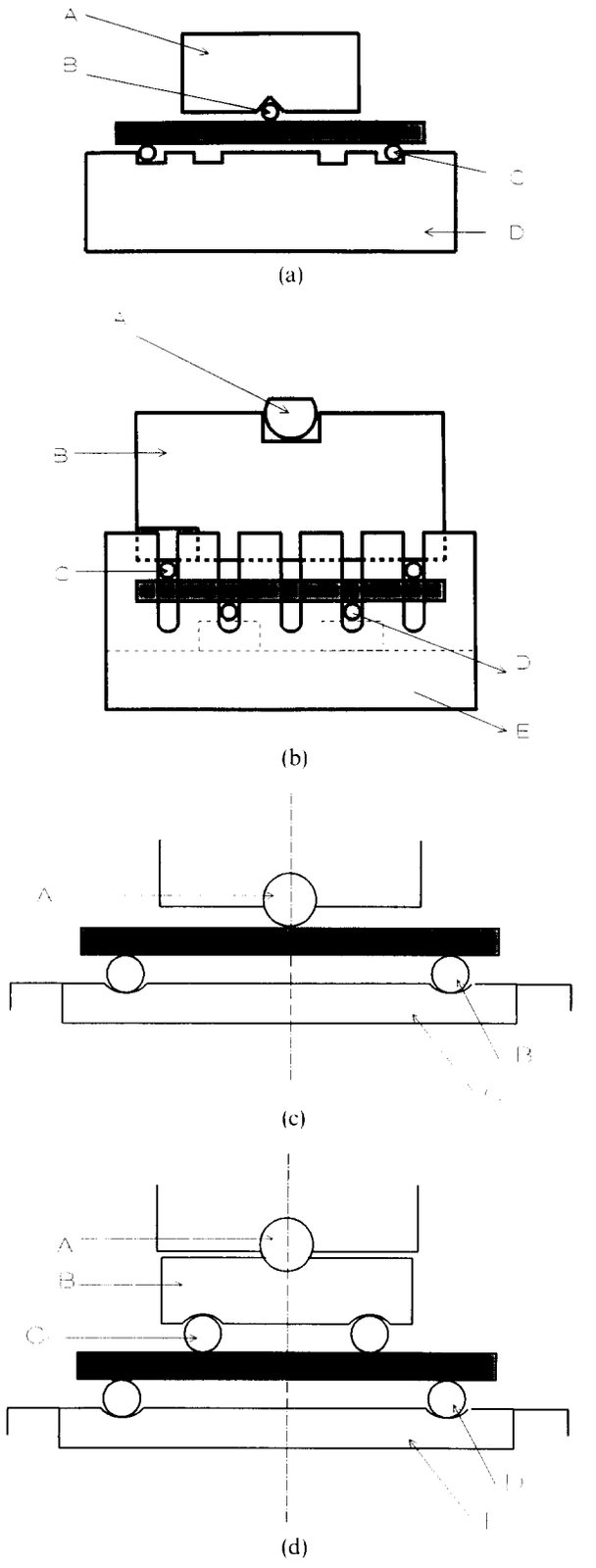


**Fig. 1.** Schematic representations of the test jigs (not to scale). Specimen is shaded. (a) Three-point bend jig (jigs A and D in text): A = alignment; B = loading roller; C = support roller; D = base-plate. (b) Four-point bend jig (jigs E and F in text): A = alignment; B = upper plate; C = loading roller; D = support roller; E = base plate. (c) Ball-on-ring jig (jig B in text): A = loading ball; B = support bearing; C = bearing race. (d) Ring-on-ring jig (jig C in text): A = loading ball of jig B; B = bearing race; C = loading bearing; D = support bearing; E = bearing race.

3 mm. Positioning of the bend bars was performed with a centring device.

The jigs E and F (Fig. 1(b)) were designed for four-point bending. These jigs were made of Nimonic and SiC respectively. The rollers of jig E had a clearance of 0·2 mm, the rollers of jig F 0·08 mm. With jig E two types of tests were performed. One test with the outer rollers placed to the inner edges and the inner rollers placed to the outer edges of the grooves, and a second test with the rollers vice versa. In the first test, the rollers were supposed to be able to move during bending, whereas they were supposed to be fixed during the second test. Since the clearance of the rollers of jig F was very small, no attention was paid to the exact roller position. For additional alignment, semi-cylindrical supports could be applied on the lower rollers in jigs E and F instead of the rectangular supports. Tests were performed on the alumina bend bar to determine the effects of these alignments. In jigs D, E and F, the deflection of the specimens could be measured with a transducer. The deflection was measured with respect to the outer rollers to compensate for displacements and deformations of the fixture.

Jig B (Fig. 1(c)) was used for ball-on-ring bending with two different disc sizes. Discs with a radius of 10 mm were tested on two different types of support rings. Firstly, the specimen was supported by 24 flat pins arranged at a ring of 6 mm in radius, secondly a ball-bearing (8 balls, 1·25 mm in radius) with a radius of 6 mm was used. For the discs with a radius of 15 mm, a ball-bearing (9 balls, 2·5 mm in radius) with a radius of 10 mm was used. The discs were centrally loaded by a steel ball with a radius of 2·5 mm. Jig B was easily converted to jig C (Fig. 1(d)) for ring-on-ring bending of discs with a radius of 15 mm. Ball-bearings with radii of 10 and 6 mm were used as support and loading ring respectively. Godfrey & John[12] have mentioned this successful application of ball-bearings before. The loading ball-bearing was positioned by the ball of jig B, centring itself into the extended ball-bearing race. In both jig B and C the discs were positioned by three alignment screws.

The specimens were made of two types of glass (borosilicate and crown glass) and a commercially available alumina (Al-997, Wesgo Division GTE Products Corp, USA). The properties of these materials are listed in Table 2. All test bars were cut from one sheet of borosilicate glass to the desired dimensions. The discs were cut from one sheet of crown glass. The specimens edges were not chamfered, with exception of the alumina bend bar. However, the chamfer of this bar was too small to cause any significant influence on the moment of

**Table 3.** Strain gauges used in the experiments

| *Number* | *Type* | *Gauge length (mm)* |
|---|---|---|
| 1[a] | KFC-1-D16-11[c] | 1·0 |
| 2[a] | KFC-0·3-C1-11 | 0·3 |
| 3[a] | KFC-1-C1-11 | 1·0 |
| 4[a] | KFC-2-C1-11 | 2·0 |
| 5[b] | EA-06-125BT-120 | 3·125 |

[a] Kyowa Electronic Instruments Co., Japan.
[b] Micro Measurements, USA.
[c] 90° Rosette (two filaments).

inertia. At the CTK, all glass bars and discs were provided with one strain gauge of various lengths in the centre of the specimen at the surface loaded in tension. All specimen–strain gauge combinations are summarized in Table 1.

For the ball-on-ring test, six specimens (three of 10 mm and three of 15 mm in radius) were also provided with strain gauge rosettes, which recorded the strain in two mutual perpendicular directions. For the ball-on-ring and the ring-on-ring measurements, the same discs were used. One disc of 15 mm in radius was provided with a rosette (type 1 in Table 3) in the centre and six strain gauges (type 2 in Table 3) located at different distances from the centre in order to measure a strain profile. The gauges were connected to a temperature-compensated Wheatstone bridge and amplifier (UPH 3200, Hottinger Baldwin Messtechnik, FRG). The position of each strain gauge was accurately measured with an optical microscope. The positional accuracy was 0·05 mm.

At the ECN, an alumina bar was provided with two parallel strain gauges (type 5 in Table 3) in the centre of the tensile specimen surface. These were also connected to a temperature-compensated Wheatstone bridge and amplifier (KW7 3073, Hottinger Baldwin Messtechnik, FRG).

At the CTK, all specimens were strained up to 900–1000 microstrain in order to minimize hysteresis prior to each measurement. The actual measurements consisted of three loading cycles up to 800–900 microstrain, during which the force and strain were measured. These were registered by means of a personal computer. The alumina bend bar was used only at the ECN. This bar was prestrained up to 135 microstrain. The measurements consisted of five loading cycles up to this strain level. The force and strain were registered by an $x$–$y$ recorder. The same procedure was applied to one of the glass bend bars, where the maximum strain level was about 500 microstrain. The crosshead speeds of all test configurations are listed in Table 2.

## 3 Results

All measurements yielded a strain–force graph, which was used for further calculations. The slopes of these graphs, $d\varepsilon/dF$, were determined by a least-squares analysis on the digital data of the CTK and manually on the analog data of the ECN. From these slopes, Young's modulus of the material was calculated. Subsequently, the deviation $\delta$ of each measurement was defined as

$$\delta = \frac{E_m - E_{pe}}{E_{pe}} \times 100 \quad (\%) \tag{1}$$

in which $E_m$ and $E_{pe}$ represent the measured Young's modulus and Young's modulus determined by the pulse-echo technique respectively.

**Table 4.** Results of three-point bend tests on glass and alumina

| *Laboratory* | *Span (mm)* | *Jig* | *N* | *Material* | $E_{bt}$ *(GPa)* | $\delta_{bt}$ *(%)* | $E_{sk}$ *(GPa)* | $\delta_{sk}$ *(%)* |
|---|---|---|---|---|---|---|---|---|
| CTK | 19·8 | A | 3 | Borosilicate glass | 62·8 | 2·0 | 61·8 | 0·4 |
| | 20·2 | A | 3 | | 62·4 | 1·2 | 61·4 | −0·4 |
| | 29·8 | A | 3 | | 61·9 | 0·5 | 61·3 | −0·5 |
| | 30·2 | A | 3 | | 61·8 | 0·3 | 61·1 | −0·7 |
| | 39·8 | A | 3 | | 62·8 | 2·0 | 62·3 | 1·2 |
| | 40·2 | A | 3 | | 62·8 | 2·0 | 62·3 | 1·2 |
| ECN | 20·0 | D | 1 | Borosilicate glass | 62·0 | 0·6 | 61·1 | −1·0 |
| | 20·4 | D | 1 | | 62·9 | 2·1 | 62·0 | 0·5 |
| | 30·0 | D | 1 | | 61·4 | −0·3 | 60·8 | −1·4 |
| | 40·0 | D | 1 | | 61·1 | −0·8 | 60·7 | −1·5 |
| | 40·4 | D | 1 | | 62·1 | 0·7 | 61·7 | −0·1 |
| | 40·0 | D | 1 | Alumina | 359·1 | −2·7 | 359·4 | −2·6 |

$N$ = Number of samples; $E_{bt}$ = Young's modulus calculated with the simple beam theory; $E_{sk}$ = Young's modulus calculated with the simple beam theory and Seewald–von Karman correction for wedging stresses.

### 3.1 Uniaxial experiments

*3.1.1 Three-point bend test*

All results of the three-point bend tests are listed in Table 4. These results take into account the deviation of the appropriate span lengths due to the clearance of the rollers in the grooves. Young's modulus was calculated according to the simple beam theory, $E_{bt}$, and according to the simple beam theory[13] in combination with the Seewald–von Karman correction, $E_{sk}$.[13,14] Since the strain gauge covered an area with a stress gradient, $E_{bt}$ was calculated applying an average value of the simple beam stress pattern in the area covered by the filament. In combination with Hooke's law, this resulted in:

$$E_{bt} = \frac{3s}{2wh^2}\left(1 - \frac{l_{sg}}{2s}\right)\frac{dF}{d\varepsilon} \tag{2}$$

in which $s$ is the span length, $l_{sg}$ the length of the strain gauge and $w$ and $h$ are the width and the height of the bar respectively (listed in Table 1).

The Seewald–von Karman correction accounts for the wedging effect in three-point bending. This wedging effect perturbs the linear stress profile and is a result of the concentrated contact force from the loading roller acting upon the bend bar. A model was proposed[12] in which a constant stress zone with span $s_2$ was assumed in the centre of the tensile surface, which can be approximated by $0{\cdot}177\,h$. For the present purpose, however, the Seewald–von Karman correction had to be averaged over the total strain gauge length, since all strain gauges overlapped this zone. In combination with Hooke's law this resulted in:

$$E_{sk} = \frac{3s}{2wh^2}\left(1 - 0{\cdot}266\frac{2h}{3s}\right)\frac{1}{l_{sg}} \times \left\{s_2 + \frac{l_{sg} - s_2}{s_2 - s}\left[\tfrac{1}{2}(l_{sg} + s_2) - s\right]\right\}\frac{dF}{d\varepsilon} \tag{3}$$

For the borosilicate glass bars, both jigs A and D yield results within the same range of accuracy. At the CTK, however, the test results of one bar yielded an anomalously high deviation in comparison with the other three bars and was therefore omitted. A possible explanation for this error could be improper gluing. With the application of the Seewald–von Karman correction, the average performance of jig A on the other three bars is within 0·7% accuracy for all span lengths. The average performance of jig D is within 0·9% accuracy. Without the Seewald–von Karman correction, the average performance is within 1·3% accuracy for jig A and 0·9% for jig D.

There is no obvious relationship between roller position in the groove and friction for jig A (see Table 4). However, Young's moduli from jig D with the rollers placed to the other edges of the grooves are consequently greater than those with the rollers placed to the inner edges (±1·5% and ±1·0% for the borosilicate glass and the alumina bend bar respectively). Young's moduli determined with jig A are systematically somewhat larger than those determined with jig D. The average result of jig D on the alumina bend bar reveals a deviation which is slightly greater (2·1%).

*3.1.2 Four-point bend test*

The results of the four-point bend tests, also differentiated to the proper span lengths, are listed in Table 5. Since, in this case, the strain gauges were situated within the constant stress zone between the inner rollers, only the stress pattern according to the beam theory was applied to calculate Young's modulus. For this purpose, the following equation was used:

$$E = \frac{3(s_1 - s_2)}{2wh^2}\frac{dF}{d\varepsilon} \tag{4}$$

where $s_1$ and $s_2$ denote the outer and inner span respectively.

**Table 5.** Results of four-point bend tests on glass and alumina

| *Laboratory* | $S_1$ (*mm*) | $S_2$ (*mm*) | *Jig* | *Material* | *N* | *E* (*GPa*) | $\delta_{bt}$ (%) |
|---|---|---|---|---|---|---|---|
| CTK | 39·8 | 20·2 | A | Borosilicate glass | 1 | 61·3 | 0·5 |
| | 40·2 | 19·8 | | | 1 | 61·0 | 1·0 |
| ECN | 40·0 | 20·0 | E | Borosilicate glass | 1 | 60·7 | −1·5 |
| | 40·4 | 19·6 | | | 1 | 62·5 | 1·5 |
| | 40·0 | 20·0 | E | Alumina | 1 | 360·5 | −2·3 |
| | 40·4 | 19·6 | | | 1 | 366·8 | −0·6 |
| | 40·0 | 20·0 | F | Alumina | 1 | 363·6 | −1·5 |

$N$ = Number of measurements; $s_1$ is the outer span length and $s_2$ is the inner span length.

Young's modulus of the borosilicate glass obtained from the four-point bend tests with jig A and E falls within 0·7 and 1·5% accuracy respectively of the pulse-echo value. For jig E the exact roller position is of more influence than for jig A. The average deviation of the alumina bend bar determined with jigs E and F was 1·5%.

### 3.2 Biaxial experiments

*3.2.1 Ball-on-ring bend test*

For the stress calculations of the axisymmetric ball-on-ring problem, it is assumed that on the surface loaded in tension both the radial and tangential stresses are equal and maximum within a zone with radius $b$ equal to one-third of the specimen thickness $t$:[5,6] $b = \frac{1}{3}t$.

This assumption is generally referred to as the 'Westergaard' approximation[5] and has been applied to larger specimens before with satisfying results.[7] Outside this equibiaxial stress zone, the stresses decrease rapidly towards the specimen support.

Except for strain gauge 1, all gauges cover an area which is larger than the constant stress zone. The gauges therefore measure the average strain over their length, which results in average values for Young's modulus, $\bar{E}_m$. A comparison with the analytical solution is nevertheless possible if the pulse-echo value is substituted in this solution and a theoretical average value for Young's modulus, $\bar{E}_{th}$, is calculated for each gauge length. In general, the radial stress, $\sigma_{rr}$, and the tangential stress, $\sigma_{tt}$ at distance $r$ are given by:

$$\sigma_{rr}, \sigma_{tt} = f(r) \tag{5}$$

where the full expression of $f(r)$ is given in the literature.[12]

The average radial stress over a line with radius $R_0$ can be written as:

$$\bar{\sigma}_{rr} = \frac{1}{R_0}\int_0^{R_0} \sigma_{rr}\,dr = \bar{\sigma}_{rr}(R_0, b) \tag{6}$$

which results in the following equations for the radial and tangential strains:

$$\bar{\varepsilon}_{rr} = \frac{\sigma_{rr} - \nu\sigma_{tt}}{E} \tag{7}$$

$$\bar{\varepsilon}_{tt} = \frac{\sigma_{tt} - \nu\sigma_{rr}}{E} \tag{8}$$

where $\nu$ denotes Poisson's ratio.

With the assumption that both radial and tangential stresses are equal, eqns (7) and (8) can be combined. Thus, the average radial strain can be written as:

$$\bar{\varepsilon}_{rr} = \frac{(1-\nu)\sigma_{max}}{\bar{E}} = \frac{1}{E}(\bar{\sigma}_{rr} - \nu\bar{\sigma}_{tt}) \tag{9}$$

where $\bar{E}$ represents the average value of Young's modulus:

$$\bar{E} = \frac{(1-\nu)\sigma_{max}E}{\bar{\sigma}_{rr} - \nu\bar{\sigma}_{tt}} \tag{10}$$

Note that in Ref. 7 the difference between $\sigma_{rr}$ and $\sigma_{tt}$ was neglected, but this did not influence the final conclusion concerning the Westergaard ($b = t/3$) approximation.

The results of this procedure are represented in Table 6 for the specimens of 10 mm and 15 mm in radius, supported at rings of 6 and 10 mm in radius respectively.

It is obvious that the measurements performed with the pin support resulted in a greater deviation compared to the ball-bearing measurements. In the latter case, deviations for the individual measurements are smaller than 2·2% with an average of 1·4%. The results of the measurements with the specimens of 15 mm in radius are similar. For each gauge length the deviation is smaller than 2%. The average deviation is less than 1·1% for both specimen sizes if a ball-bearing is used as a specimen support.

The measurements with the rosettes were used to check the alignment of the experimental set-up for

**Table 6.** Results of ball-on-ring tests on crown glass, calculated for $b = t/3$ (see text for further explanation)

| *R (mm)* | *a (mm)* | *Gauge length (mm)* | | | | | | $\bar{\delta}$ |
|---|---|---|---|---|---|---|---|---|
| | | *L = 0·3* | | *L = 1·0* | | *L = 2·0* | | |
| | | $\delta$ | *N* | $\delta$ | *N* | $\delta$ | *N* | |
| 10 | 6 PS | −2·5 | 3 | −6·9 | 3 | −7·6 | 3 | −5·7 |
| 10 | 6 BS | 2·2 | 3 | −0·4 | 3 | −1·6 | 3 | 0·1 |
| 15 | 10 BS | 1·7 | 3 | 0·7 | 3 | 1·0 | 3 | 1·1 |

PS = pin support; BS = ball-bearing support; $R$ = specimen radius; $a$ = support radius; $L$ = gauge length; $N$ = number of measurements; $\bar{\delta}$ = average deviation.

both the 10 and 15 mm specimens. Since these gauges record the strain in two mutual perpendicular directions, the coefficient of the slope of a $\varepsilon_1 - \varepsilon_2$ graph should be 1. With the least-squares analysis the average slope was calculated from three measurements for both set-ups. The deviation is defined analogously as before. For the specimens of 15 mm in radius, an average coefficient of 1·04 was calculated. For the specimen of 10 mm in radius the corresponding result is 1·002, indicating an acceptable alignment for both set-ups.

An attempt was made to measure a strain profile over the tensile surface of a 15 mm specimen. The deviations from theory at different distances $r$ from the specimen centre are listed in Table 7. Since the strain is nearly negligible at large distances from the centre, the results are considered to be in good agreement.

*3.2.2 Ring-on-ring bend test*

In the case of coaxial loading of a disc by two rings of different radius which are both smaller than the disc, an equibiaxial stress zone arises at the tensile specimen surface within the smaller ring. Eight strain gauge measurements were carried out in order to determine Young's modulus. Additionally, two measurements were done to test the axisymmetry of the set-up. Since the stress is constant within the inner loading ring, Young's modulus can be calculated directly with the thin plate solution[9] and the stress–strain relationship for a biaxial stress state, resulting in:

$$E = \frac{3(1-\nu^2)}{2\pi t^2}\frac{\mathrm{d}F}{\mathrm{d}\varepsilon} \left\{\ln\left(\frac{a}{b}\right) + \frac{(1-\nu)}{(1+\nu)}\left(\frac{a}{R}\right)^2\left[\frac{1}{2} - \frac{1}{2}\left(\frac{b}{a}\right)^2\right]\right\} \quad (11)$$

Here, $a$ is the radius of the outer ring, $b$ is the radius of the inner ring, and $R$ and $t$ are the disc radius and thickness respectively. Table 8 lists the results of these experiments in terms of the average deviation (as defined before) from pulse-echo Young's modulus.

**Table 7.** Deviations of the theoretical strain profile, measured at different distances $r$ from the specimen (15 mm in radius, 1 mm in thickness) centre for the ball-on-ring test on crown glass

| *r (mm)* | *δ (%)* |
|---|---|
| 3·01 | 10·0 |
| 3·33 | 10·0 |
| 4·00 | −4·0 |
| 4·39 | 8·0 |
| 4·80 | −39·0 |
| 5·56 | 16·0 |

**Table 8.** Results of the ring-on-ring tests on crown glass

| *Gauge length* | *N* | $\bar{\delta}$ (%) |
|---|---|---|
| 0·3 | 2 | 0·3 |
| 1·0 (rosette) | 4 | 0·6 |
| 1·0 | 3 | 0·7 |

$N$ = Number of measurements, $\bar{\delta}$ = average deviation.

Young's modulus was also calculated from the measurements with the rosettes.

For all gauge lengths the deviation is less than 1%. However, one of the measurements with the 0·3 mm strain gauges yielded a deviation of 7%. Since the specimen failed during the experiment, the origin of this error could not be traced and the measurement was not taken into account. The measurements with the rosettes were used to determine the axisymmetry, analogously as described above for the ball-on-ring test. The average coefficient $\mathrm{d}\varepsilon_1/\mathrm{d}\varepsilon_2$ was 1·015, again indicating an acceptable alignment.

## 4 Discussion and Conclusions

Strain gauges offer a powerful tool if one is in doubt of the accuracy of stress calculations from forces in bending tests. This accuracy depends largely on the amount of friction at specimen–support and specimen–load contacts. Two uniaxial bend tests (three-point bending at different span lengths and four-point bending) and two biaxial bend tests (ball-on-ring and ring-on-ring) have been analysed. All tests yielded acceptable results, on average about 1% accuracy.

The main experimental condition for accurate bending is the presence of specimen supports which are able to move and thus reduce frictional errors to a minimum. In the case of the uniaxial tests this condition is realized by free rollers in oversized flat grooves. The results of the deflection measurements on the alumina and the glass bar are not presented in this report but it is worthwhile mentioning an important observation. It appeared that the strain gauge measurement was significantly influenced by the spring force (±1 N) of the deflection measurement system. Although this force seems negligible, it results in a systematic error within the load range used of both the borosilicate glass (maximum force about 70 N) and the alumina (maximum force about 120 N) bar. Furthermore, random errors were introduced by the lateral shift of the deflection pins, resulting in irreproducible measurements. Therefore it was recommended not to apply the system in strength tests.

One might argue whether the use of the pulse-echo

values as reference values for the elastic moduli is correct. From the bend resonance method, however, the same values were obtained within 1% accuracy for both glass and alumina. The data from the deflection measurements agreed as well, within the errors mentioned before. Therefore the pulse-echo values can be taken as reference for the materials used in the the analysis.

Promising results regarding axisymmetry and frictionless bending in the biaxial tests were achieved by the application of ball-bearings. They offer a successful alternative for solid rings, which contribute a significant amount of friction into the bending system. Even discontinuous resilient rings suffer this problem, and should therefore be omitted. On the other hand, accurate positioning of both the specimen and the test jig is a prerequisite.

Shetty *et al.*[6] mentioned the stress concentration at the loading ring in ring-on-ring testing. The magnitude of this concentration however, is strongly dependent on the test geometry. Finite element method calculations with the geometry used in this work have shown that the magnitude is less than 1%. Nevertheless, it has to be accounted for when interpreting strength data obtained with the ring-on-ring set-up. Whether the satisfying ball-bearing application for the biaxial tests can also be used for the development of an accurate high-temperature ball-on-ring and ring-on-ring test facility, will be evaluated in further research. For ball-on-ring bending, the Westergaard approximation for the radius of the constant stress zone is allowed for the experimental dimensions used in this work.

When calculating the stress from the applied load, one has to be aware of the wedging effect in three-point bending. If this is taken into account by using the Seewald–von Karman correction, it is sufficiently corrected for. In general, the desired experimental accuracy for bending tests at room temperature has been achieved. Thus, Weibull parameters obtained from strength tests will be less biased. Results from strength tests performed at the two laboratories can be directly compared. Moreover, the prediction of the biaxial strength of a ceramic from uniaxial data can be better experimentally verified, as demonstrated in the accompanying paper.

## Acknowledgements

The authors wish to thank J. M. Ijzermans (Department of Mechanical Engineering, Eindhoven University of Technology) and N. v.d. Burg and M. Jong (Netherlands Energy Research Foundation) for their assistance during all measurements and manufacturing the specimens. The work in this paper has partly been sponsored by the Commission Innovative Research Program Technical Ceramics (IOP-TK) of the Ministry of Economic Affairs in the Netherlands (IOP-TK research grant 88.B040).

## References

1. Quinn, G., Flexure strength of advanced structural ceramics: a round robin. *J. Am. Ceram. Soc.*, **73** (1990) 2374–94.
2. Baratta, F. I., Quinn, G. D. & Matthews, W. T., Errors associated with flexure testing of brittle materials. US Army Materials Technology Laboratory, MTL TR 87-35, 1987.
3. Newnham, R. C., Strength tests for brittle materials. *Proc. Brit. Ceram. Soc.*, **25** (1975) 281–93.
4. Hoagland, R. G., Marschall, C. W. & Duckworth, W. H., Reduction of errors in ceramic bend tests. *J. Am. Ceram. Soc.*, **59** (1975) 189–92.
5. Westergaard, H. M., Stresses in concrete pavements computed by theoretical analysis. *Public Roads*, **7** (1926) 25–35.
6. Shetty, D. K., Rosenfield, A. R., McGuire, P., Bansal, G. K. & Duckworth, W. H., Biaxial flexure test for ceramics. *Am. Ceram. Soc. Bull.*, **59** (1980) 1193–7.
7. de With, G. & Wagemans, H. H. M., Ball-on-ring test revisited. *J. Am. Ceram. Soc.*, **72** (1989) C1538–C1541.
8. Fessler, H. & Fricker, D. C., Multiaxial strength tests for brittle materials. *J. Strain Analysis*, **19** (1984) 197–208.
9. Fessler, H. & Fricker, D. C., A theoretical analysis of the ring-on-ring loaded disk test. *J. Am. Ceram. Soc.*, **67** (1984) 582–8.
10. Marshall, D. B., An improved biaxial flexure test for ceramics. *Am. Ceram. Soc. Bull.*, **59** (1980) 551–3.
11. Dortmans, L. & de With, G., Noise sensitivity of fit procedures for Weibull parameter extraction. *J. Am. Ceram. Soc.*, **74** (1991) 2293–4.
12. Godfrey, D. J. & John, S., Disc flexure tests for the evaluation of ceramic strength. In *Proceedings of the International Conference Ceramic Materials for Components and Engines*, ed. W. Bunk & H. Hausner. DKG, Berlin, 1986, pp. 657–65.
13. Timoshenko, S. P. & Goodier, J. N., *Theory of Elasticity*. 3rd edn, McGraw-Hill, London, 1970.
14. Diaz, G. & Kittl, P., On the Seewald–Karman correction in fracture statistics of a rectangular beam. *Res. Mechanica*, **24** (1988) 209–18.